Materials Discovery 1 (2015) 10–20

Contents lists available at ScienceDirect

Materials Discovery

journal homepage: www.elsevier.com/locate/md

Review

Multimodal imaging of harmonophores and application of high content imaging for early cancer detection

Anuraag Boddupalli [a], Kaitlin M. Bratlie [a,b,c,*]

[a] Department of Chemical & Biological Engineering, Iowa State University, Ames, IA 50011, United States
[b] Department of Materials Science & Engineering, Iowa State University, Ames, IA 50011, United States
[c] Ames National Laboratory, Ames, IA 50011, United States

ARTICLE INFO

Article history:
Received 10 August 2015
Received in revised form
19 November 2015
Accepted 19 November 2015
Available online 22 December 2015

Keywords:
Second harmonic generation
Collagen
Cancer
Image analysis
Nonlinear optics

ABSTRACT

Multimodal imaging techniques aim to improve the efficiency of current cancer diagnostic methods and provide greater insight into the tumour microenvironment. Second harmonic generation microscopy (SHG) is a non-destructive imaging technique available to researchers for detecting the changes in the morphology of collagen. Researchers aim to understand the role played by changes in collagen morphology in tumour development. Hybrid imaging methods are able to combine the specificity of collagen detection by SHG with other narrow ranged fluorescent or biochemical markers, leading to higher efficiency of cancer diagnosis and grading. Different cancer diagnoses have been detected efficiently by these methods, with higher clarity than standard protocols. Higher contrast between malignant and normal tissue, achieved using high content imaging using SHG, have also allowed for development of non-invasive follow-up of cancer treatment methods. The aim of this review is to provide an overview of the analysis techniques currently used to further improve the efficiency of cancer detection.

Contents

* Corresponding author at: Department of Materials Science & Engineering, Iowa State University, Ames, IA 50011, United States.
E-mail address: kbratlie@iastate.edu (K.M. Bratlie).

http://dx.doi.org/10.1016/j.md.2015.11.002
2352-9245/

1. Introduction

The latest reports from the National Cancer Initiative show that Cancer has grown to become the 2nd largest cause for death in the United States, behind only heart disease. Beyond the emotional trauma suffered by families across countries worldwide, cancer also has a very high economic impact on countries all over the world [1,2]. A recent study by the Agency for Healthcare Research and Quality estimated that $88.7 billion were spent just over 4 years back in 2011. With the rising costs, and the fragile state of the economy, cancer has progressed in importance and there remains a need for immediate action, in spite of mortality trends suggesting that the situation has improved, as can be seen in Fig. 1.

Multimodal imaging has sought to provide early diagnosis and a better understanding for several of the fast acting types of cancers that are becoming a common fixture of the health-care sector. Techniques such as second harmonic generation (SHG) microscopy have provided researchers a hybrid imaging technique which can offer biochemical insights into clinical samples, and yield information on a multitude of tumour diagnoses. SHG imaging uses two incoming photons having the same wavelength, scatter after interacting with a chiral molecule, and produce one photon of exactly half the incoming wavelength. The most important characteristics of imaging collagen or other SHG-active biomolecules, are to firstly consider their ability to polarize the incident laser beams, due to their non-centrosymmetric structure. The second takeaway point from SHG imaging is that the technique is very sensitive to changes in molecular orientation, which is especially valid for 3-D structures. The aforementioned variables lead to a major difference in the data analysis, when considering the conformal changes between different types of collagen, as it influences the tensor ratios obtained which are sensitive to the density and conformations of collagen [3,4] (Fig. 2).

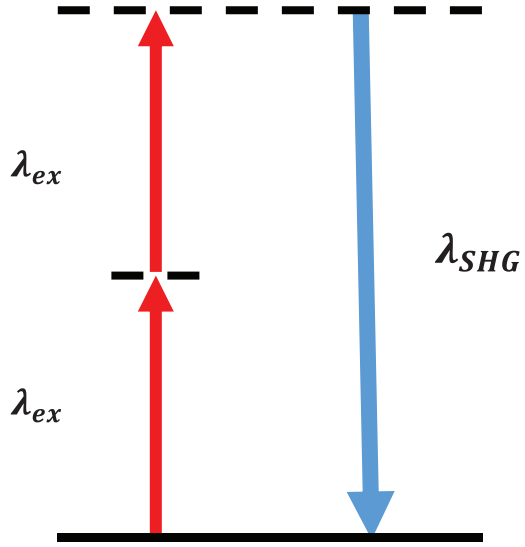

Fig. 2. Jablonski diagram representing the excitation of two near infrared photons, into a single visible photon of double the wavelength in an SHG setup.

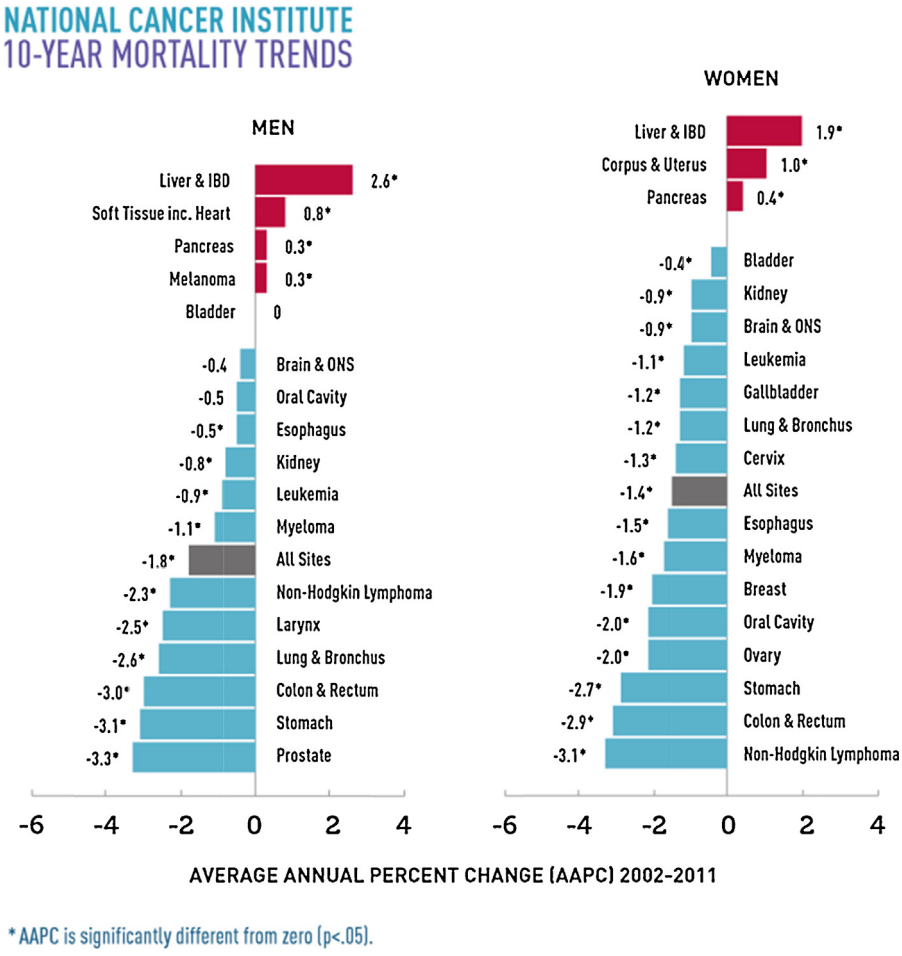

Fig. 1. Latest cancer trends report indicating the mortality rate of cancer in different types of cancer and their mortalities in men and women [1].

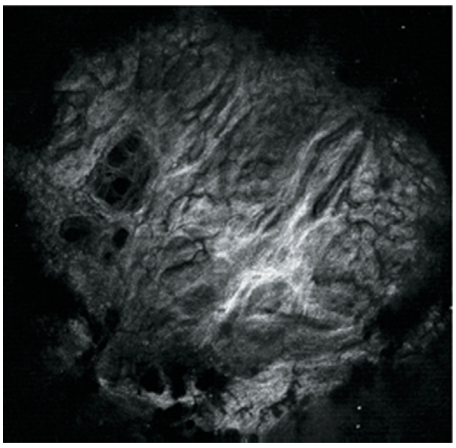

Fig. 3. SHG image of a melanoma growth in sub-dermal tissue of a mouse. Image width was 6.6 mm [12]. Reproduced with permission.

SHG imaging has been shown to have many advantages over traditional immunohistochemistry staining techniques or fluorescence microscopy. It is a non-linear optical approach towards imaging tissues both in situ as well as being a part of endomicroscopy approaches [5–7]. The SHG imaging approach is a non-staining, energy conservative technique. This is most suitable for non-destructive imaging of tissues, while simultaneously allowing for the internal visualization of the samples be clear. The most important prerequisite condition for SHG-active sites within the tissues is therefore to be a non-centrosymmetric salient component within, which are selectively detected by the incident beam. Common examples of SHG active molecules, known as harmonophores are collagen types I and III, myosin (when present within actomyosin complexes), and cholesterol crystals (ChC) which are chiral in nature [8–10].

Studies conducted by Su et al. [11] have shown that extracellular matrix (ECM) alterations are a very important indicator for different kinds of tumour growth within corneal, colonic, cardiac, breast, and ovarian tissues. Intensity based SHG imaging can yield clear images of the modifications of the tissue structure, by elucidating collagen orientation changes in the ECM, as can be seen in Fig. 3, which is an image taken of a sub-dermal tumour in a mouse, from the studies conducted by Brown et al. [12].

The most common challenge in methods such as SHG are that there is a complex amount of data generated for each tissue imaging, based on the fact that the harmonophores show varying intensity with polarization of the incident beams. These intensities, measurements of the forward, backward-scattering beams, and the variations of the angular pitch of the harmonophores necessitate a need for detailed analysis of the data generated. A significant concurrence needs to be achieved for the understanding of the results generated by this field of high content imaging.

2. State of the art

It is interesting to note that the discovery of SHG as an imaging tool was by accident, and a consequence of experiments carried out to expand their knowledge in piezoelectricity. Two young researchers Fukada and Yasuda, who were working on a piece of Achilles tendon observed a macroscopic polarity to the sample. This polarity was hypothesized to be a consequence of charged repeating groups in crystal form, which was further confirmed by Lang a few years later [13]. Together these observations created the breakthrough which allowed for biological molecules having chiral symmetry be visualized in a non-linear manner, without compromising the structural or chemical integrity of the samples. One of the first examples shown to be easily differentiated on the basis of SHG imaging were rat tail tendons and trachea cartilage, as they both contain collagen, but of different types [11]. These studies were gradually improved on to image differences in collagen morphology in mouse ovary, skin and bone samples [14].

It was observed that combining SHG with techniques such as two photon excitation fluorescence (TPEF) microscopy or coherent anti-Stokes Raman spectroscopy (CARS) can help provide biochemical specificity to the tissues being imaged. With the help of additional, non-destructive non-linear optics, further information about cancers such as basal cell carcinoma (BCC) were readily available, as shown by Vogler's group in 2010 [15]. The presence of fat reservoirs, collagen modifications, and fluorescing proteins was visualized by this multimodal imaging technique (as seen in Fig. 4), providing new insight into BCC, which is an extremely fast acting cancer with a high mortality rate, as observed by Jemal's study in 2008 [16]. These studies further made the case for high content imaging to be popularized all over the world. Fig. 4 elucidates how different imaging techniques used for identifying specific biochemical or structural signatures, such as collagen detected by SHG microscopy and CARS showing the fat reservoirs in the cancer tissue can be linked together to provide a holistic view of how malignant tissues metabolize nutrients and later metastasize. These studies further made the case for high content imaging, to be popularized all over the world, in order to provide an early detection system for spread of cancer tissue [17–19].

As demonstrated for BCC, dermal tissues were one of the first imaged using SHG due to the ease of access and availability of samples [20,21]. Chen and his group, showed SHG and TPEF as a viable hybrid imaging tool [22], by simultaneously imaging collagen and elastin respectively. There was a clear difference observed in how the scars and normal dermis showed different levels of elastin and collagen presence.

Cicchi et al. demonstrated in 2010 how structurally different hypertrophic scarring in keloids is from healthy dermis at the micron scale [9,23]. It was observed that normal dermis contained a randomly mixed presence of collagen and elastin, whereas keloids showed well aligned boundaries of collagen with very minimal presence of elastin. As keloids are present only in humans [22,24,25], and the nature of keloids have been shown to be influenced by melanin content, studies such as these hold great promise in the fields of tissue engineering. These studies were further substantiated by independently analysing the orientation of the collagen fibres formed, through fast Fourier transform (FFT) analysis. It was clear the isotropic nature of collagen fibres in keloids matched well with the visual observations made previously by Su et al. in 2011 [21,23,25–27].

The success of SHG imaging spurred interest in the early detection of breast cancer. In order to understand the significant difference between the clarity of tissue sections, Ambekar compared the haematoxylin & eosin stained (H&E) sections with the collagen mapped using SHG [28]. The sensitivity of SHG in detecting changes in collagen morphology has proved to be a game changer for this aspect of breast cancer detection at an early stage, as shown in Fig. 5. As seen below, the SHG imaging clearly marks the regions of interest where collagen alteration is taking place in the cancer tissue, thereby showing the relation between its conformations, which can contribute towards developing tumour biomarkers using SHG. Several groups such as Brown, Burke, Conklin, and Ajeti have defined aspects of breast cancer types based on SHG [20,29,31,32].

The process of ECM modifications in cartilage and mammary tissues was studied in depth by Burke and co-workers in 2015 [29,30]. In their studies they aimed to provide visual confirmation of the hypothesis put forward by Conklin in 2011 [31] regarding

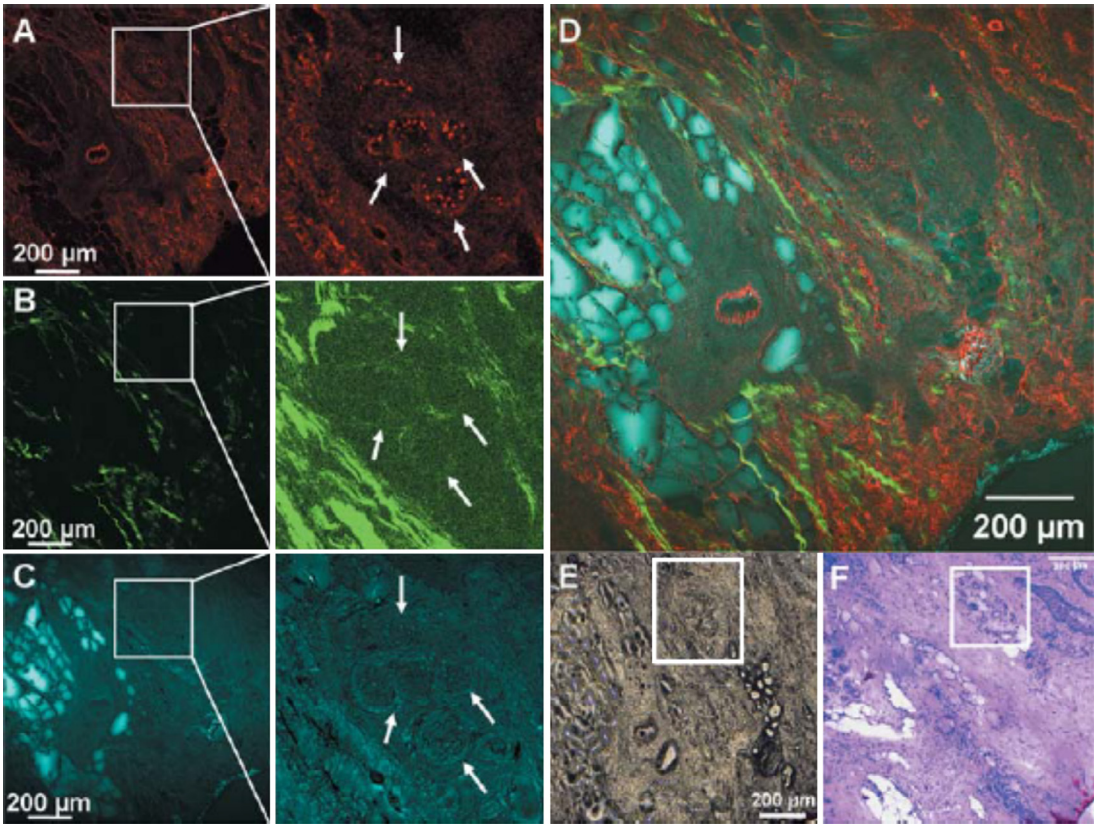

Fig. 4. (A) TPEF highlighting the fluorescing proteins in the tissue, (B) SHG indicating the collagen organization around the carcinoma, (C) CARS showing the fat reservoirs around the carcinoma, (D) hybrid image of all three techniques, (E) brightfield image of the carcinoma, (F) H&E staining of the tissue to provide perspective, with insets highlighted for imaging [15]. Copyright Wiley-VCH Verlag GmbH & Co. KgaA. Reproduced with permission.

how collagen fibres re-align themselves from a randomly ordered state to that of a structured form, as evidenced by the their imaging of mammary tumours which is shown in Fig. 6. Conklin defined his theory on tumour associated collagen signatures (TACs) on this basis, which we shall delve into later during this review. Here too, SHG imaging agrees with the standard pathology of improve the early diagnosis, detection of breast cancer.

Another salient example of the application of SHG in cancer detection was towards the diagnosis of liver fibrosis. By combining TPEF with SHG, clear SHG-fibrosis indices were established, which

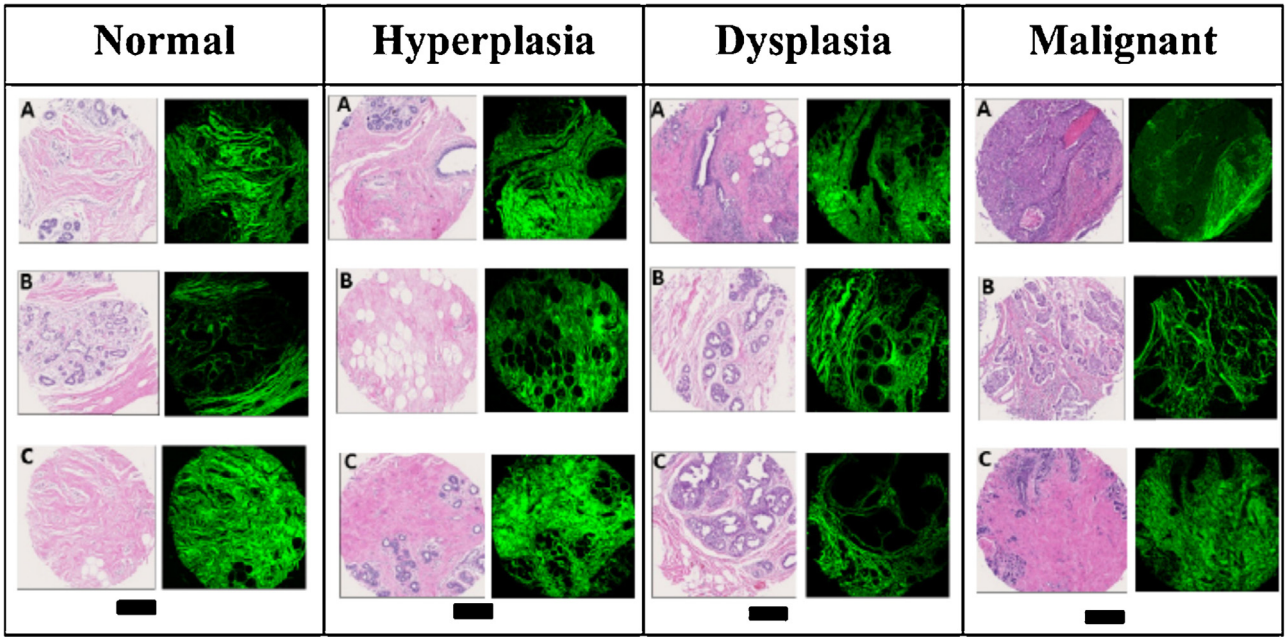

Fig. 5. H&E and SHG imaging comparison for grades of breast cancer tissues [29]. Reproduced with permission.

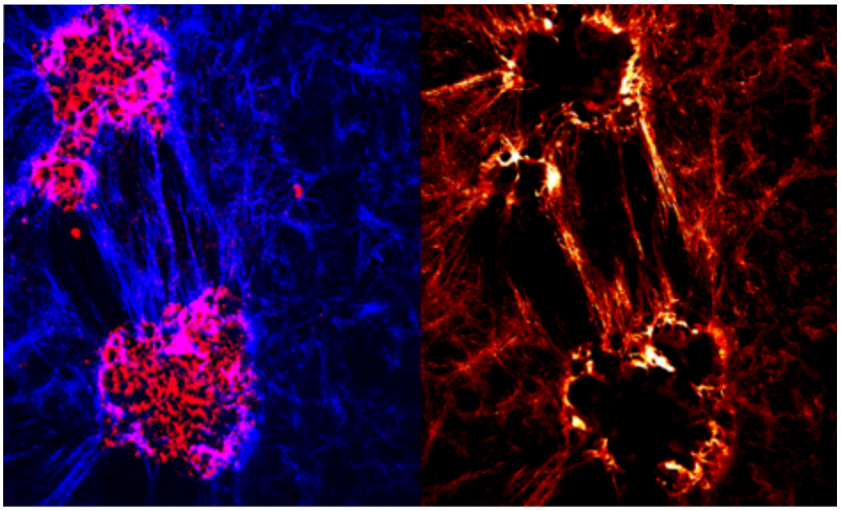

Fig. 6. (left, red) Collagen organization at the onset of breast cancer, (left, blue) collagen alignment three days after onset. Changes in the forward and backward scattering of SHG signal [30]. Reproduced with permission. (For interpretation of the references to colour in this figure legend, the reader is referred to the web version of this article.)

were confirmed by the Metavir scoring of fibrosis [33,34]. This correlation of fibrosis indices, developed by Gailhouste in 2011[35] is further vindication of the multimodal imaging process, using SHG and TPEF as a hybrid imaging platform, which also elucidates the difference in the mechanisms between the two methods [36].

3. Analysis techniques

It is essential to understand that advanced imaging techniques such as SHG, two photon microscopy (TPM) and CARS are highly customizable. It is often up to the researcher to determine what data to extract from the imaging and how best to represent it in a coherent and effective way. The most common forms of data produced are from intensity measurements taken from sectioning the polarized images of the samples. There are also methods by which certain patterns in the alignment of the detected signal can be detected through MATLAB codes, producing statistical data comparing different regions of interest (ROIs) on the samples. These multimodal imaging techniques can produce vast amounts of data for a single image, and we will summarize the most common analysis techniques used by researchers all over the world [37–39].

The growing requirement for quantitative SHG imaging resulted in the development of techniques which are used primarily for cancer detection and classification studies. The analysis techniques listed in this section progress from the most intrinsic data analysis that can be directly done from the SHG intensity data, such as that obtained from susceptibility measurements, polarized imaging profiles, and forward/backward SHG (F/B SHG) methods. Further techniques are explained such as second harmonic to autofluorescence ageing index of dermis (SAAID), depth dependence decay (DDD), and grey local correlation matrix (GLCM) which are those that have been developed from specific cancer studies and provide a different perspective on understanding the SHG component of hybrid imaging techniques. We have given below some of the salient analysis methods observed.

3.1. Susceptibility measurements (χ ratios)

The SHG signal obtained for any collagen containing sample is characterized by the second order nonlinear susceptibility tensor $\chi^{(2)}$. The relationship between the susceptibility, the electrical field applied (E) and the polarization (P) is defined as:

$$P_{ijk} = \chi_{ijk} E_j E_k \tag{1}$$

For small molecules, it is understood that the main contributors to the susceptibility values are the C═O and the N—H groups present in the amide bonds [40]. Hence, this tensor is indicative of the collagen directionality within the imaged domains. For ease of analysis as well as approximation based on the point sized light source and the sample thickness not exceeding 5 μm, we consider the samples to observe cylindrical symmetry and follow the Kleinmann rules. The relation thus shall exhibit only two independent components: χ_{XXX} and $\chi_{XYY} = \chi_{XZZ} = \chi_{YXY} = \chi_{ZXZ} = \chi_{YYX} = \chi_{ZXX}$ where X is the direction of the collagen fibrils [4,27].

An incident electric field E_0 then induces the following second harmonic wave in the fibril frame XYZ:

$$E_X^{2\omega} \propto [\chi_{XXX} \cos^2(\alpha - \varphi) + \chi_{XXX} \sin^2(\alpha - \varphi)] E_0^2 \tag{2a}$$

$$E_Y^{2\omega} \propto [\chi_{XYY} \sin 2(\alpha - \varphi)] E_0^2 \tag{2b}$$

In the above equations, α and φ stand for the laser excitation polarization angle and the fibril orientation angle, respectively, with respect to a fixed direction in the laboratory frame, usually taken as the X axis which is considered here to be the collagen fibril axis. This is valid because the lamellae within the collagen shall be parallel to the axis, and hence within plane of the electrical field E_0. The total polarized collagen intensity is then given by:

$$I^{2\omega} = K|\rho \cos^2(\alpha - \varphi) + \sin^2(\alpha - \varphi)|^2 + |\sin 2(\alpha - \varphi)|^2 \tag{3}$$

In the above equation, K is a constant merging the squared incident intensity and setup geometrical parameters. Two quantitative parameters appear in this expression: (i) the angle difference of α and φ, of the laser excitation polarization to the collagen fibrils axis within lamellar domains; (ii) the ratio ρ, which reflects the anisotropy of the nonlinear response of these lamellar domains, and is calculated as $\rho = \chi_{XXX}/\chi_{XYY}$. This approach to calculate the polarization anisotropy (ρ) and susceptibility (P) is valid for both forward scattered SHG as well as backward scattered SHG signals [22].

In some cases, where the methylene contribution is considered separately, some of the above assumptions do not hold true for all the tensor elements. Some cases studies and theoretical models show the polarizability of the sample denoted by β in such cases, resulting in the system being defined by three related elements:

$$\chi_{XXX} = N^{(p)} \beta^{(p)} \cos^3 \theta^{(p)} + N^{(m)} \beta^{(m)} \cos \theta^{(m)} \tag{4a}$$

$$\chi_{XYY} = \frac{1}{2} N^{(p)} \beta^{(p)} \cos \theta^{(p)} \sin^2 \theta^{(p)} \tag{4b}$$

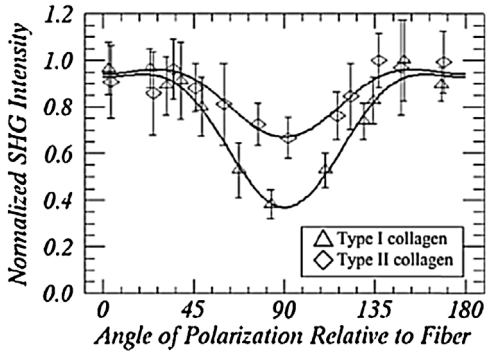

Fig. 7. Normalized SHG intensity observed relative to the polarization angle [11]. Reprinted from [11]. Copyright (2010), with permission from Elsevier.

$$\chi_{YYX} = \frac{1}{2}N^{(p)}\beta^{(p)}\cos\theta^{(p)}\sin^2\theta^{(p)} + N^{(m)}\beta^{(m)}\cos\theta^{(m)} \quad (4c)$$

In these above equations, $N^{(p)}$ and $N^{(m)}$ refer to the number of peptide and methylene groups in the system respectively. And the $\theta^{(p)}$ represents the pitch angle to which the collagen is oriented, and accordingly determined as per the following equations:

$$a = \chi_{XXX}/\chi_{XYY} \quad \text{and} \quad b = \chi_{YYX}/\chi_{XYY}$$

and

$$\tan^2\theta^{(p)} = \frac{2}{a-b+1} \quad (5)$$

Studies conducted by Su et al. [11] on cartilage imaging relied on using these equations and susceptibility ratios in order to characterize differences between collagen type I and type II in rats, as shown in Fig. 7 [27,35,41].

Su et al., also demonstrated a clear change in intensity observed with respect to change in polarization. They highlighted one of the first examples of collagen morphologies being different in tendons and cartilage tissues, with the change in morphology from wavy, random signals to well aligned fibres.

3.2. Polarization resolved SHG imaging

As the intensity of the SHG signal obtained for collagen presence is dependent on not just the concentration, but also the degree of ordering of the fibres, spacing, and the overall anisotropy of the collagen in the samples, this approach can be taken up in multiple applications, such as on the basis of the polarization anisotropy, or as separate measurements for each incident polarization angle. On the basis of polarization anisotropy, the image intensities were normalized over the following equation [42]:

$$PA = \frac{I_{||} - I_{\perp}}{I_{||} + I_{\perp}} \quad (6)$$

Here, the $I_{||}$ values were for those with horizontal polarization and $I_{\perp}$ values for the vertically polarized imaging. PA values of 0 signify a high order of stochasticity, and those tending towards 1 or −1 are more uniaxial in orientation.

Polarization resolved imaging studies were conducted by Ambekar et al., to observe the differences in the intensity [28] for different incident polarization angles (from 0° to 180°), in various stages of breast cancer tissues [5,8,27]. This differentiation based on polarization was further elucidated by mapping the anisotropy of each of the 4 samples.

3.3. Fast Fourier transform analysis (FFT)

The images obtained by SHG microscopy can be analysed using an FFT based model where each image is divided into user-defined regions of interest, according to which each part of the image is fit through an elliptical model [43]. The major and minor axis of this ellipse define the orientation of the collagen fibre within the ROI. Optimized ROIs are used in order to define the best collagen resolution, and obtain an orientation map. The shapes of the collagen fibres are first approximated to that of an ellipse, and the FFT analysis further estimates the centroid of the ROI, and calculates the distance of each point in the fibre from the centroid in order to obtain an overall orientation angle using radial vectors which sweep over 360° from the *X*-axis [44].

Tan et al. [43] analysed porcine cornea samples using FFT, and obtained clearly demarcated orientation lines for different regions of the sample in Fig. 8.

Akilbekova et al. used the FFT analysis in order to obtain resolved orientations of the collagen in the samples [45]. They were able to obtain shape description values for each of the samples, showing the different overall distribution of the collagen, differentiating between systems where the collagen was well-aligned to those which showed a random distribution [8,31].

3.4. F/B ratio measurements

Another analysis technique used the nature of SHG measurements having a forward and backward scattering component, hitherto referred as F-SHG and B-SHG respectively. It has been understood that the F-SHG imaging is extremely sensitive to the presence of large collagen bundles which are of the order of the magnitude of the incoming SHG signal, whereas the B-SHG is sensitive to the septa and interstices created by randomly distributed small deposits of collagen, where the forward signal gets collected, but the backward signal is propagated stronger. The ratio of these two area percentages or intensities observed in the samples is often denoted as the F/B ratio, and taken as measure of the evolution of collagen alterations in the sample [46].

For each of the sample images, a stack is created, where a threshold is applied such that the signal to noise ratio is optimized for the individual F-SHG and B-SHG measurements. This threshold is used to create a mask, where all the non-collagen areas are automatically allotted a null value, with the collagen areas having value of 1. This sort of binary differentiation of the images brings the signal to the highest clarity. Depending on the types of cancer or tissue studied, the area percentage or the average intensity values are measured for each image in the F-SHG stack and divided by the corresponding images for the B-SHG one [47].

Groups such as Latour et al. [41] took additional care to ensure the validity of such measurements by polarization resolving F/B ratio studies. As collagen is known to be anisotropic, they were able to obtain even higher resolutions of the stromae observed in cornea samples, this analysis was combined with the direction maps created for the collagen alignment.

Another method of representing F/B ratio data is through statistically calculating the difference in the ratios, observed for different types of healthy and cancer tissues [46]. Many different types of non-parametric testing such as the Newman–Keuls test, help calculate the standard deviation and variances without compromising the integrity of the data. Kottman et al., recently published their work on understanding the alteration in the ECM [48] as observed in different lung cancer tissues. Here, they studied an early detection strategy to differentiate between a highly invasive cryptogenic organizing pneumonia (COP) from usual interstitial pneumonia (UIP) and healthy tissue. UIP is characterized usually by a decrease in lung volume and non-productive cough, and is a common yet highly serious medical condition amongst smokers. UIP or idiopathic pulmonary fibrosis (IFP) patients often need to undergo lung transplantation after diagnosis. On the other hand, COP can be characterized by the presence of granular buds in the alveoli

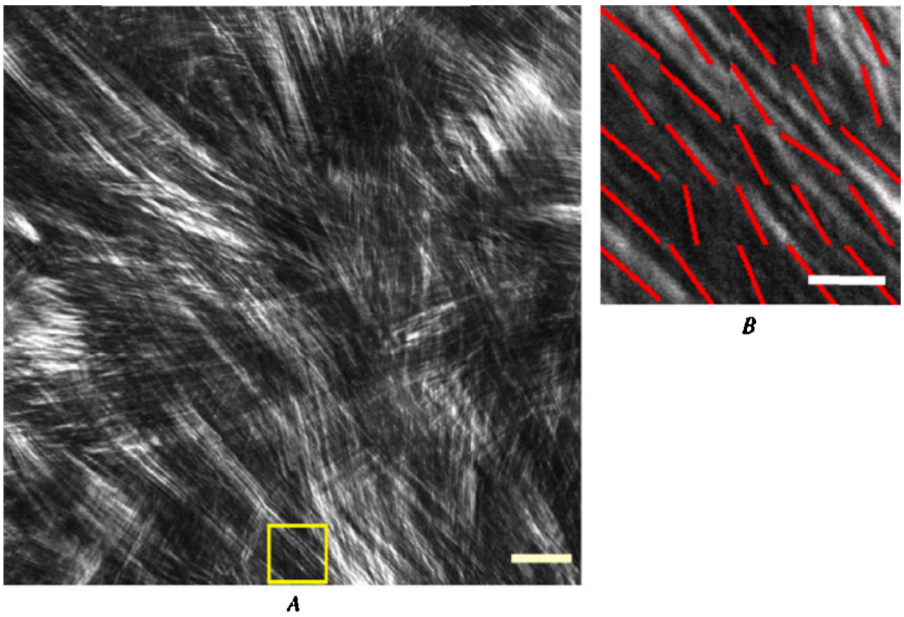

Fig. 8. (A) Large area of porcine cornea (scale: 40 μm); (B) collagen orientation lines mapped for the yellow inset box based on FFT analysis (scale: 10 μm) [43]. Reprinted from [43]. Copyright (2013), with permission from Elsevier.

and bronchioles. Most cases of COP are cured within three months of treatment with corticosteroids unlike for UIP, where such treatments are largely ineffective [49,50]. In cases such as these, an early detection method such as SHG F/B ratio analysis can potentially avoid fatalities.

3.5. Grey local correlation matrix

Grey local correlation matrix (GLCM) is a statistical method to analyse texture in greyscale images [51]. It analyses each ROI, with relation to its neighbouring areas. This method can be set to analyse the images even on a pixel by pixel basis, by changing the offset, accounting for different channels within the image.

It can be classified largely on the basis of three applications:

a. On the basis of weighted means which are multiplied to the GLCM values depending on distance from the main diagonal:
   i. For analysing dissimilarity (D) where the weights multiplied to the GLCM values increase as you move away from the diagonal

$$\sum_{i,j=0}^{N-1} P_{i,j}\left|i-j\right| \tag{7}$$

   ii. For analysing contrast (C) where the weights multiplied to the GLCM values decrease as you move away from the diagonal, also known as sum of squares variance.

$$\sum_{i,j=0}^{N-10} P_{i,j}(i-j)^2 \tag{8}$$

   iii. For analysing homogeneity (H) where the weights multiplied to the GLCM values decrease exponentially as you move away from the diagonal. This is most applicable to images having a high contrast range.

$$\sum_{i,j=0}^{N-1} \frac{P_{i,j}}{1+(i-j)^2} \tag{9}$$

b. On the basis of spatial matrix values, complete measurements based on orderliness. Similar to contrast wise measurements, orderliness measures are calculated with GLCM weighted averages on the basis that:
   iv. Weights that increase with commonness shall increase with orderliness
   v. Weights that decrease with commonness shall increase with disorder

   The three orderliness measures defined under the GLCM theory are:
   - ASM or Energy mean which can be calculated by the following equation typically for cases where the matrix is highly orderly.

$$\sum_{i,j=0}^{N-1} P_{i,j}^2$$

   - Max Probability (MAX): Simply records the highest value of the matrix in the centre.
   - Entropy measurement based completely on the disorderliness of the system, and calculated by:

$$\sum_{i,j=0}^{N-1} P_{i,j}(-\ln P_{i,j})$$

c. On the basis of statistics, calculating the GLCM mean, median and variance The correlation (R) of each pixel to its neighbouring ones are calculated as: In these equations, the expectation values are denoted by μ and the standard deviations are denoted by σ.

$$R = \sum_{i,j} \frac{(i-\mu_i)(j-\mu_j)p_{i,j}}{\sigma_i \sigma_j} \tag{10a}$$

$$\mu_i = \sum_{i=1}^{N} i.p_{i,j}; \quad \mu_j = \sum_{i=1}^{N} i.p_{i,j} \tag{10b}$$

$$\sigma_i = \sqrt{\frac{1}{N-1}.\sum_{i=1}^{N} i.p_{i,j}}; \quad \sigma_j = \sqrt{\frac{1}{N-1}.\sum_{i=1}^{N} j.p_{i,j}} \tag{10c}$$

By modifying the offset values and studying the correlation, more information about the texture can be measured, as the offset directly influences the distance between each neighbouring ROI taken into consideration. Cicchi et al. [23] did important work on imaging and understanding the structural differences between keloids and normal human dermis using the GLCM data analysis techniques. On the basis of calculating the homogeneity, correlation, and energy for different ROI values, they obtained a clear trend to tell apart normal dermis samples from excessively scarred keloid tissue.

3.6. Second harmonic to autofluorescence ageing index of dermis (SAAID)

In the field of dermatology, it became necessary to be able to image collagen for a variety of applications. Tissue engineering [9,23,42] also benefited from the studies conducted on quantifying the collagen density, especially when it could give more information on the proportions of elastin present alongside it. Such multimodal imaging studies were carried out by researchers all over the world, where SHG was combined with any autofluorescence imaging technique which targeted the elastin present in the tissue samples.

SAAID has been devised as a measure of the collagen fibre intensity based on the hybrid TPEF imaging done along with SHG. The combined intensity values are used to calculate SAAID as per the following formula:

$$\text{SAAID} = \frac{I_{\text{SHG}} - I_{\text{TPEF}}}{I_{\text{SHG}} + I_{\text{TPEF}}} \tag{11}$$

It can be used as a measure of the collagen to elastin ratio in the dermal samples, as the elastin can be tagged with TPEF-active fluorescent markers, and the SHG will specifically only show collagen density. The SAAID is a very useful tool hence to determine the difference between normal skin, keloids and normal scars. As humans are the only mammals who exhibit the presence of keloids in response to physical trauma or at times of surgery [21,52], this analysis technique helps evaluate the tendency of certain tissues to develop to the keloids stage, where the elastin is significantly higher than for normal skin or scars.

Using this notation, the SAAID value hence approaches -1 when the collagen present in the sample is completely replaced by the elastin. In 2014, Cicchi et al. [42], used the SAAID values to evaluate the effectiveness of laser ablative treatment in removing scarred tissue from normal dermis. In this study, they evaluated over three age groups of patients. Group I consisted of those less than 35 years of age, Group 2 were between 35 and 60, whereas the last group were above 60. Their images and results indicated clear differences in the amounts of collagen and elastin present, after multimodal imaging pre and post laser treatment [9,23].

The results showed clearly that the SAAID values for normal skin was close to −1 due to the high presence of elastin, whereas the scores for keloids and scar tissues were closed to 1 owing to the higher concentration of collagen in the samples. The SAAID value measurements are often accompanied in every study by two-sample parametric test, to be sure of statistical differences observed for the different sample types and also evaluate the standard deviation and means.

3.7. Depth dependant decay measurements

In order for techniques such as SHG and TPEF to be comparably applicable to imaging different kinds of tumours, research groups devised the depth dependent decay (DDD) studies analysis method, which helps quantify the SHG signal differing from the change in the focal plane. It was observed that the signal intensity would exponentially increase with the increase in depth, and such a system could be easily represented by a first order equation where 'x' represented the imaging depth, and 'y' represented the SHG collagen intensity. For such systems, A is the pre-exponential scaling factor, C is the proportionality constant which ensures the non-collagen areas to have a null value [22,53,54]:

$$y = Ae^{-kx} + C \tag{12}$$

The k value obtained from the above equation is the DDD factor which is completely dependent on the sample absorption and composition. The collagen intensities can be easily obtained against the different focal plane depths, and extrapolated as per the exponential equation to obtain the k values for different samples.

Many groups such as Chen et al. [22] in Taiwan have studied the differences between cartilage, tendons, and normal skin using SHG. They applied the DDD model to identify the difference between hypertrophic scars and normal dermis in this study from 2009.

These DDD studies can also be utilized for differentiating between collagen mixtures of different proportions due the sensitivity of the k values observed. Ajeti et al. [32] used the DDD study to identify how collagen type I and V showed very different absorption and scattering properties, the results of which could go a long way in analysing different artificial tissue samples and their preparation.

4. Different cancer staging methods

Imaging methods such as SHG, have been shown to have a significant number of advantages over traditional cancer scoring systems. The different data analysis approaches that can be applied to the SHG data provide greater details about the sample [56], and at the same time, they do not damage the sample or use stains of any kind. It is essential though to see how the standard scoring systems can be combined with SHG analysis to provide concurrence for cancer diagnoses. The American Joint Committee on Cancer (AJCC) [60] compiles information and, along with the International Union against Cancer (UICC), concurs on the classification of different cancer staging processes, as it is not a straightforward process, which varies widely within particular cancer diagnoses. The motivation behind the different scoring system remains to provide information on the severity of the cancer diagnosis, and allows oncologists and researchers to identify the next steps in the cancer treatment processes. AJCC provides thus a ready reference for classifying different stages of cancer and, in the context of high content imaging, allows for the identification of cancer markers. Most importantly though, these scoring systems provide for a connection between the hybrid imaging and clinical data obtained from oncological research, which clarifies how SHG imaging can become an important tool for tumour characterization. We shall discuss below, some commonly used oncological scoring systems:

4.1. Metavir Scoring system

In this system, the severity of the liver cancer diagnosis, observed through histopathological examination of a liver biopsy, is made on the basis of two levels [33,34]. Firstly on the basis of inflammation, where it is graded from A0 to A4-ranging from 'no activity' to 'severe activity'. And secondly on the basis of the stage of fibrosis observed as:

- F0—No fibrosis
- F1—Portal fibrosis without septa
- F2—Portal fibrosis with few septa
- F3—Numerous septa without cirrhosis
- F4—Cirrhosis

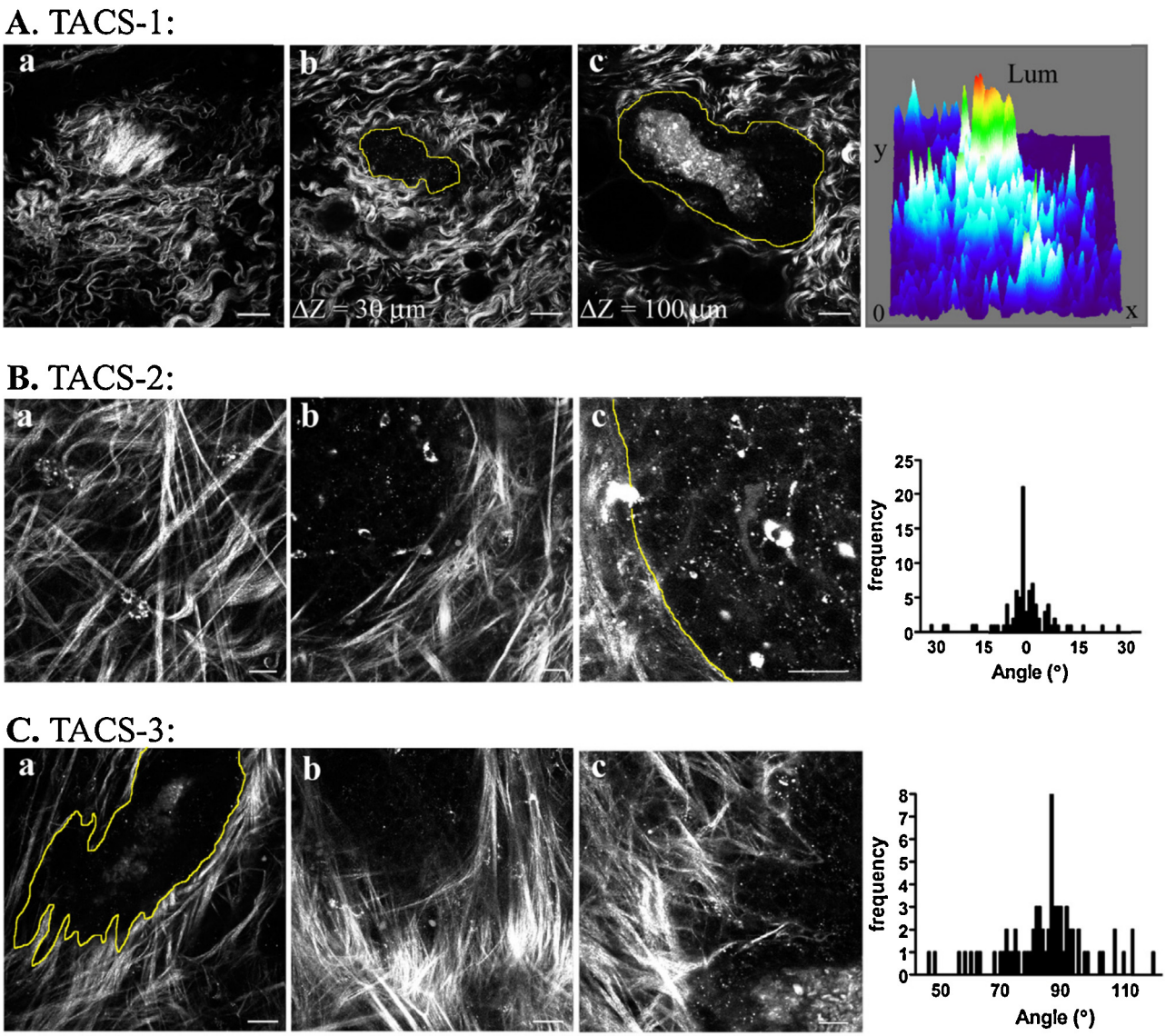

Fig. 9. Tumour associated collagen signature types in A, B, C, along with associated bar graph profiles for intensity of collagen signatures for that TACS orientation [57].

4.2. TNM system

The TNM system for classifying severity of cancer is one of the most commonly accepted and used to differentiate between different stages of cancer. Unlike the Metavir Scoring system, the TNM scoring applies to a wide range of cancer diagnoses.

In this system, each letter signifies a different key characteristic of the cancer diagnosis [55]. Starting with T, which denotes the size and hence reach of the primary tumour. For invasive cancer types, it is essential to know whether the cancer has spread to the nearby lymph nodes, and is denoted by N. And lastly, M denotes whether the cancer has spread to other parts of the body, forming secondary tumours in a process defined as metastasis-denoted by M. The values assigned to each of the letters can hence reveal a lot of information about the cancer diagnosis in a short, clear manner.

For the primary tumour (T) classifications, TX represents that the tumour could not be evaluated. T0 indicates the absence of the primary tumour, whereas T shows that the tumour is non-invasive at this stage. T1, T2, T3 and T4 all denote the size of the tumour.

In the regional lymph nodes (N) scoring, similarly NX represents non-evaluable tumour presence lymph node, N0 shows absence of tumour in the nodes. And N1, N2 and N3 denote the severity of the lymph node involvement, indicating the number of lymph nodes affected.

For the metastasis (M) scoring, MX shows that the metastasis could not be evaluated, M0 denotes absence of the invasiveness, and M1 shows its presence [56].

4.3. Tumour associated collagen signatures (TACS)

For the purpose of understanding and defining key characteristics observed in collagen morphologies in cancer tissues, Provenzano et al. [57] introduced the nomenclature of TACS. Studies had shown that in the cases of hyperplasia, adenocarcinoma and ductal carcinoma observed in mice, there were consistent epithelial clusters surrounded by an increased presence of collagen. These collagen morphologies were observed to always be one of three types, which helped classify the severity and invasiveness of the cancer diagnosis in the subjects [31].

- TACS 1-is recognized by highly dense and intense signal imaged for the small tumour detected.

- TACS 2-is recognized by a smooth tumour boundary, within which the collagen fibres are majorly aligned parallel to the tumour boundary.
- TACS 3-is recognized by collagen fibres being tangentially or perpendicularly aligned to the tumour boundary.

Fig. 9 from the study conducted by Keeley, shows the visual differences between the three TACS classifications.

5. Future perspectives and conclusions

Positive trends have been observed for many of the cancer detection techniques, which have shown that these multimodal imaging techniques using SHG in combination with TPEF or CARS, have concurred with the standard pathology in place. This is a very important step in the establishment of protocol for early cancer detection, which shall improve the quality of living for the families affected by these deadly diseases [57], which are often based on genetic traits.

We have discussed the varied applications of SHG and the different high content imaging approaches towards cancer research [57–59]. It is evident that these methods produce highly complex data, and it thus requires the need for big data analysis. Over the course of our survey of the latest work using SHG analysis, we tried to observe certain trends and preferences for using set techniques for the treatment of data, but it was very difficult to do so. Consensus established for optimized methods of testing which satisfy researchers across borders can help in global benefits. A possible step forward to this goal would be to encourage inter-disciplinary research projects to combat cancer types in laboratories and universities across the world. With the advancements, in the field of analytics, it would surely not be very long before non-parametric testing of data [59] as recommended in this review become the norm. Thereby reducing any bias of the data, based on the technique themselves, and establishing concurrence sooner with the existing clinical pathologies.

Acknowledgements

This work was supported by the National Science Foundation under Grant No. CBET 1227867, the Roy J. Carver Charitable Trust Grant No. 13-4265, and the Mike and Denise Mack faculty fellowship to KB.

References

[1] American Cancer Society, Cancer Facts & Figures 2015, Atlanta, GA, 2015.
[2] L. Rahib, B.D. Smith, R. Aizenberg, A.B. Rosenzweig, J.M. Fleshman, L.M. Matrisian, Projecting cancer incidence and deaths to 2030: the unexpected burden of thyroid, liver, and pancreas cancers in the United States, Cancer Res. 74 (11) (2014) 2913–2921, http://dx.doi.org/10.1158/0008-5472.CAN-14-0155.
[3] K. Burke, P. Tang, E. Brown, Second harmonic generation reveals matrix alterations during breast tumor progression, J. Biomed. Opt. 18 (3) (2013) 31106, http://dx.doi.org/10.1117/1.JBO.18.3.031106.
[4] A. Golaraei, R. Cisek, S. Krouglov, R. Navab, C. Niu, S. Sakashita, V. Barzda, Characterization of collagen in non-small cell lung carcinoma with second harmonic polarization microscopy, Biomed. Opt. Express 5 (10) (2014) 3562, http://dx.doi.org/10.1364/BOE.5.003562.
[5] H. Bao, A. Boussioutas, R. Jeremy, S. Russell, M. Gu, Second harmonic generation imaging via nonlinear endomicroscopy, Opt. Express 18 (2) (2010) 1255–1260, http://dx.doi.org/10.1364/OE.18.001255.
[6] Y. Zhang, M.L. Akins, K. Murari, J. Xi, M.-J. Li, K. Luby-Phelps, M. Mahendroo, X. Li, A compact fiber-optic SHG scanning endomicroscope and its application to visualize cervical remodeling during pregnancy, Proc. Natl. Acad. Sci. U.S.A. 109 (32) (2012) 12878–12883, http://dx.doi.org/10.1073/pnas.1121495109.
[7] D.R. Rivera, C.M. Brown, D.G. Ouzounov, I. Pavlova, D. Kobat, W.W. Webb, C. Xu, Compact and flexible raster scanning multiphoton endoscope capable of imaging unstained tissue, Proc. Natl. Acad. Sci. U.S.A. 108 (43) (2011) 17598–17603, http://dx.doi.org/10.1073/pnas.1114746108.
[8] J.L. Suhalim, C.-Y. Chung, M.B. Lilledahl, R.S. Lim, M. Levi, B.J. Tromberg, E.O. Potma, Characterization of cholesterol crystals in atherosclerotic plaques using stimulated Raman scattering and second-harmonic generation microscopy, Biophys. J. 102 (8) (2012) 1988–1995, http://dx.doi.org/10.1016/j.bpj.2012.03.016.
[9] R. Cicchi, C. Matthäus, T. Meyer, A. Lattermann, B. Dietzek, B.R. Brehm, B.R. Popp, F.S. Pavone, Non-linear imaging and characterization of atherosclerotic arterial tissue using combined two photon fluorescence, second-harmonic generation and CARS microscopy, Multiphot. Microsc. Biomed. Sci. XIV 9329 (2014) 894807, http://dx.doi.org/10.1117/12.2037018.
[10] H. Liu, W. Qin, Y. Shao, Q. Liu, Z. Ma, T.K. Borg, B.Z. Gao, Live cardiomycyte imaging via hybrid TPEF–SHG microscopy, Proc. SPIE 8225 (2012), http://dx.doi.org/10.1117/12.908381, 822524–7.
[11] P.J. Su, W.L. Chen, T.H. Li, C.K. Chou, T.H. Chen, Y.Y. Ho, C.H. Huang, S.J. Chang, Y.Y. Huang, H.S. Lee, C.Y. Dong, The discrimination of type I and type II collagen and the label-free imaging of engineered cartilage tissue, Biomaterials 31 (36) (2010) 9415–9421, http://dx.doi.org/10.1016/j.biomaterials.2010.08.055.
[12] E. Brown, T. McKee, E. diTomaso, A. Pluen, B. Seed, Y. Boucher, R.K. Jain, Dynamic imaging of collagen and its modulation in tumors in vivo using second-harmonic generation, Nat. Med. 9 (6) (2003) 796–800, http://dx.doi.org/10.1038/nm879.
[13] I. Freund, M. Deutsch, A. Sprecher, Optical second-harmonic microscopy, crossed-beam summation, and small-angle scattering in rat-tail tendon, Biophys. J. 50 (1986) 693–712.
[14] X. Chen, O. Nadiarynkh, S. Plotnikov, P.J. Campagnola, Second harmonic generation microscopy for quantitative analysis of collagen fibrillar structure, Nat. Protoc. 7 (4) (2012) 654–669, http://dx.doi.org/10.1038/nprot.2012.009.
[15] N. Vogler, T. Meyer, D. Akimov, I. Latka, C. Krafft, N. Bendsoe, K. Svanberg, B. Dietzek, J. Popp, Multimodal imaging to study the morphochemistry of basal cell carcinoma, J. Biophoton. 3 (10–11) (2010) 728–736, http://dx.doi.org/10.1002/jbio.201000071.
[16] A. Jemal, R. Siegel, E. Ward, Y. Hao, J. Xu, T. Murray, M.J. Thun, Cancer statistics, 2008, CA. Cancer J. Clin. 58 (2) (2008) 71–96, http://dx.doi.org/10.3322/CA.2007.0010.
[17] S. Seidenari, F. Arginelli, C. Dunsby, P. French, K. König, C. Magnoni, M. Manfredini, C. Talbot, G. Ponti, Multiphoton laser tomography and fluorescence lifetime imaging of basal cell carcinoma: morphologic features for non-invasive diagnostics, Exp. Dermatol. 21 (11) (2012) 831–836, http://dx.doi.org/10.1111/j.1600-0625.2012.01554.x.
[18] S. Seidenari, F. Arginelli, S. Bassoli, J. Cautela, A.M. Cesinaro, M. Guanti, D. Guardoli, C. Magnoni, M. Manfredini, G. Ponti, K. König, Diagnosis of BCC by multiphoton laser tomography, Skin Res. Technol. 19 (1) (2013) 297–304, http://dx.doi.org/10.1111/j.1600-0846.2012.00643.x.
[19] S. Heuke, N. Vogler, T. Meyer, D. Akimov, F. Kluschke, H.-J. Röwert-Huber, J. Lademann, B. Dietzek, J. Popp, Detection and discrimination of non-melanoma skin cancer by multimodal imaging, Healthcare 1 (1) (2013) 64–83, http://dx.doi.org/10.3390/healthcare1010064.
[20] C.-K. Sun, C.-C. Chen, S.-W. Chu, T.-H. Tsai, Y.-C. Chen, B.-L. Lin, Multiharmonic-generation biopsy of skin, Opt. Lett. 28 (24) (2003) 2488–2490, http://dx.doi.org/10.1364/OL.28.002488.
[21] M. Lilledahl, M. Olderøy, A. Finnøy, K. Olstad, J.E. Brinchman, Second harmonic generation imaging in tissue engineering and cartilage pathologies, Proc. SPIE 9329 (2015) 93291C, http://dx.doi.org/10.1117/12.2081583.
[22] G. Chen, J. Chen, S. Zhuo, S. Xiong, H. Zeng, X. Jiang, R. Chen, S. Xie, Nonlinear spectral imaging of human hypertrophic scar based on two-photon excited fluorescence and second-harmonic generation, Br. J. Dermatol. 161 (1) (2009) 48–55, http://dx.doi.org/10.1111/j.1365-2133.2009.09094.x.
[23] R. Cicchi, D. Kapsokalyvas, V. De Giorgi, V. Maio, A. Van Wiechen, D. Massi, T. Lotti, F.S. Pavone, Scoring of collagen organization in healthy and diseased human dermis by multiphoton microscopy, J. Biophoton. 3 (1–2) (2010) 34–43, http://dx.doi.org/10.1002/jbio.200910062.
[24] H.A. Linares, C.W. Kischer, M. Dobrkovsky, D.L. Larson, The histotypic organization of collagen of the hypertrophic scar in humans, J. Investig. Dermatol. 59 (4) (1972) 323–332.
[25] R.S. English, P.D. Shenefelt, Keloids and hypertrophic scars, Dermatol. Surg. 25 (8) (1999) 631–638, http://dx.doi.org/10.1046/j.1524-4725.1999.98257.x.
[26] C. Thrasivoulou, G. Virich, T. Krenacs, I. Korom, D.L. Becker, Optical delineation of human malignant melanoma using second harmonic imaging of collagen, Biomed. Opt. Express 2 (5) (2011) 1282–1295, http://dx.doi.org/10.1364/BOE.2.001282.
[27] P.J. Su, W.L. Chen, Y.F. Chen, C.Y. Dong, Determination of collagen nanostructure from second-order susceptibility tensor analysis, Biophys. J. 100 (8) (2011) 2053–2062, http://dx.doi.org/10.1016/j.bpj.2011.02.015.
[28] R. Ambekar, T.-Y. Lau, M. Walsh, R. Bhargava, K.C. Toussaint, Quantifying collagen structure in breast biopsies using second-harmonic generation imaging, Biomed. Opt. Express 3 (9) (2012) 2021, http://dx.doi.org/10.1364/BOE.3.002021.
[29] R.M. Burke, K.S. Madden, S.W. Perry, M.L. Zettel, E.B. Brown, Tumor-associated macrophages and stromal TNF-α regulate collagen structure in a breast tumor model as visualized by second harmonic generation, J. Biomed. Opt. 18 (8) (2013) 86003, http://dx.doi.org/10.1117/1.JBO.18.8.086003.
[30] K.A. Burke, R.P. Dawes, M.K. Cheema, D.S.W. Benoit, S.W. Perry, E. Brown, Second-harmonic generation scattering directionality predicts tumor cell motility in collagen gels, J. Biomed. Opt. 20 (5) (2015), http://dx.doi.org/10.1117/1.JBO.20.5.051024, 051024-1–051024-9.
[31] M.W. Conklin, J.C. Eickhoff, K.M. Riching, C. Pehlke, A.K.W. Eliceiri, P.P. Provenzano, A. Friedl, P.J. Keely, Aligned collagen is a prognostic signature for survival in human breast carcinoma, Am. J. Pathol. 178 (3) (2011) 1221–1232, http://dx.doi.org/10.1016/j.ajpath.2010.11.076.

[32] V. Ajeti, O. Nadiarnykh, S.M. Ponik, P.J. Keely, K.W. Eliceiri, P.J. Campagnola, Structural changes in mixed Col I/Col V collagen gels probed by SHG microscopy: implications for probing stromal alterations in human breast cancer, Biomed. Opt. Express 2 (8) (2011) 2307–2316, http://dx.doi.org/10.1364/BOE.2.002307.
[33] T. Poynard, P. Bedossa, P. Opolon, Natural history of liver fibrosis progression in patients with chronic hepatitis C, Lancet 349 (9055) (1997) 825–832.
[34] P. Bedossa, D. Dargère, V. Paradis, Sampling variability of liver fibrosis in chronic hepatitis C, Hepatology 38 (6) (2003) 1449–1457.
[35] L. Gailhouste, Y. Grand, C. Le Odin, D. Guyader, B. Turlin, F. Ezan, Y. Désille, T. Guilbert, A. Bessard, C. Frémin, G. Baffet, Fibrillar collagen scoring by second harmonic microscopy: a new tool in the assessment of liver fibrosis, J. Hepatol. 52 (3) (2010) 398–406, http://dx.doi.org/10.1016/j.jhep.2009.12.009.
[36] M. Strupler, A.-M. Pena, M. Hernest, P.-L. Tharaux, J.-L. Martin, E. Beaurepaire, M.-C. Schanne-Klein, Second harmonic imaging and scoring of collagen in fibrotic tissues, Opt. Express 15 (7) (2007) 4054–4065, http://dx.doi.org/10.1364/OE.15.004054.
[37] H.G. Breunig, M. Weinigel, R. Bückle, M. Kellner-Höfer, J. Lademann, M.E. Darvin, W. Sterry, K. König, Clinical coherent anti-Stokes Raman scattering and multiphoton tomography of human skin with a femtosecond laser and photonic crystal fiber, Laser Phys. Lett. 10 (2) (2013) 025604, http://dx.doi.org/10.1088/1612-2011/10/2/025604.
[38] V. Hovhannisyan, A.P.J. Su, S.J. Lin, C.Y. Dong, Quantifying thermodynamics of collagen thermal denaturation by second harmonic generation imaging, Appl. Phys. Lett. 94 (23) (2009) 2007–2010, http://dx.doi.org/10.1063/1.3142864.
[39] T. Meyer, M. Chemnitz, M. Baumgartl, T. Gottschall, T. Pascher, C. Matthäus, B.F. Romeike, B.R. Brehm, J. Limpert, A. Tünnermann, J. Popp, Expanding multimodal microscopy by high spectral resolution coherent anti-Stokes Raman scattering imaging for clinical disease diagnostics, Anal. Chem. 85 (14) (2013) 6703–6715, http://dx.doi.org/10.1021/ac400570w.
[40] S.V. Plotnikov, A.C. Millard, P.J. Campagnola, W.A. Mohler, Characterization of the myosin-based source for second-harmonic generation from muscle sarcomeres, Biophys. J. 90 (2) (2006) 693–703, http://dx.doi.org/10.1529/biophysj.105.071555.
[41] G. Latour, I. Gusachenko, L. Kowalczuk, I. Lamarre, M. Schanne-Klein, In vivo structural imaging of the cornea by polarization-resolved second harmonic microscopy, Biomed. Opt. Express 3 (1) (2012) 1, http://dx.doi.org/10.1364/BOE.3.000001.
[42] R. Cicchi, D. Kapsokalyvas, M. Troiano, P. Campolmi, C. Morini, D. Massi, G. Cannarozzo, T. Lotti, F.S. Pavone, In vivo non-invasive monitoring of collagen remodelling by two-photon microscopy after micro-ablative fractional laser resurfacing, J. Biophoton. 7 (11–12) (2014) 914–925, http://dx.doi.org/10.1002/jbio.201300124.
[43] H.Y. Tan, Y.L. Chang, W. Lo, C.M. Hsueh, W.L. Chen, A. Ghazaryan, P.S. Hu, T.H. Young, S.J. Chen, A.C.Y. Dong, Characterizing the morphologic changes in collagen crosslinked-treated corneas by Fourier transform-second harmonic generation imaging, J. Cataract Refract. Surg. 39 (5) (2013) 779–788, http://dx.doi.org/10.1016/j.jcrs.2012.11.036.
[44] T. Chen, M.J. Hilton, E.B. Brown, M.J. Zuscik, H.A. Awad, Engineering superficial zone features in tissue engineered cartilage, Biotechnol. Bioeng. 110 (5) (2013) 1476–1486, http://dx.doi.org/10.1002/bit.24799.
[45] D. Akilbekova, K.M. Bratlie, Quantitative characterization of collagen in the fibrotic capsule surrounding implanted polymeric microparticles through second harmonic generation imaging, PLOS ONE 10 (6) (2015) e0130386, http://dx.doi.org/10.1371/journal.pone.0130386.
[46] Q. Peng, S. Zhuo, P.T.C. So, H. Yu, Improving liver fibrosis diagnosis based on forward and backward second harmonic generation signals, Appl. Phys. Lett. 106 (8) (2015) 083701, http://dx.doi.org/10.1063/1.4913907.
[47] O. Nadiarnykh, R.B. LaComb, M.A. Brewer, P.J. Campagnola, Alterations of the extracellular matrix in ovarian cancer studied by second harmonic generation imaging microscopy, BMC Cancer 10 (2010) 94, http://dx.doi.org/10.1186/1471-2407-10-94.
[48] R.M. Kottmann, J. Sharp, K. Owens, P. Salzman, G.-Q. Xiao, R.P. Phipps, P.J. Sime, E.B. Brown, S.W. Perry, Second harmonic generation microscopy reveals altered collagen microstructure in usual interstitial pneumonia versus healthy lung, Respir. Res. 16 (1) (2015) 1–13, http://dx.doi.org/10.1186/s12931-015-0220-8.
[49] J.F. Cordier, Cryptogenic organising pneumonia, Eur. Respir. J. 28 (2) (2006) 422–446, http://dx.doi.org/10.1183/09031936.06.00013505.
[50] J.P. Lynch 3rd, R. Saggar, S.S. Weigt, D.A. Zisman, E.S. White, Usual interstitial pneumonia, Semin. Respir. Crit. Care Med. 27 (6) (2006) 634–651, http://dx.doi.org/10.1055/s-2006-957335.
[51] J. Linke, G.J. McDermid, A.D. Pape, A.J. McLane, D.N. Laskin, M. Hall-Beyer, S.E. Franklin, The influence of patch-delineation mismatches on multi-temporal landscape pattern analysis, Landsc. Ecol. 24 (2) (2009) 157–170, http://dx.doi.org/10.1007/s10980-008-9290-z.
[52] R. Rudolph, Wide spread scars, hypertrophic scars, and keloids, Clin. Plast. Surg. 14 (2) (1987) 253–260, PMID:3581659.
[53] S. Zhuo, J. Yan, G. Chen, H. Shi, X. Zhu, J. Lu, J. Chen, S. Xie, Label-free imaging of basement membranes differentiates normal, precancerous, and cancerous colonic tissues by second-harmonic generation microscopy, PLoS ONE 7 (6) (2012) 4–7, http://dx.doi.org/10.1371/journal.pone.0038655.
[54] S. Zhuo, X. Zhu, G. Wu, J. Chen, S. Xie, Quantitative biomarkers of colonic dysplasia based on intrinsic second-harmonic generation signal, J. Biomed. Opt. 16 (12) (2011) 120501, http://dx.doi.org/10.1117/1.3659715.
[55] S.W. Perry, R.M. Burke, E.B. Brown, Two photon and second harmonic microscopy in clinical and translational cancer research, Ann. Biomed. Eng. 40 (2) (2012) 277–291, http://dx.doi.org/10.1007/s10439-012-0512-9.
[56] L.H. Sobin, I.D. Fleming, TNM classification of malignant tumors, fifth edition (1997), Cancer 80 (9) (1997) 1803–1804, http://dx.doi.org/10.1002/(SICI)1097-0142(19971101)80:9<1803::AID-CNCR16>3.0.CO;2-9.
[57] P.P. Provenzano, K.W. Eliceiri, J.M. Campbell, D.R. Inman, J.G. White, P.J. Keely, Collagen reorganization at the tumor–stromal interface facilitates local invasion, BMC Med. 4 (1) (2006) 38, http://dx.doi.org/10.1186/1741-7015-4-38.
[58] X. Jiang, J. Zhong, Y. Liu, H. Yu, S. Zhuo, J. Chen, Two-photon fluorescence and second-harmonic generation imaging of collagen in human tissue based on multiphoton microscopy, Scanning 33 (1) (2011) 53–56, http://dx.doi.org/10.1002/sca.20219.
[59] J.W. Birk, M. Tadros, K. Moezardalan, O. Nadyarnykh, F. Forouhar, J. Anderson, P. Campagnola, Second harmonic generation imaging distinguishes both high-grade dysplasia and cancer from normal colonic mucosa, Dig. Dis. Sci. 59 (7) (2014) 1529–1534, http://dx.doi.org/10.1007/s10620-014-3121-7.
[60] American Joint Committee on Cancer, 2015, Chicago, IL, 2015.